Method for Generating High Purity Laguerre–Gaussian Vortex Modes

Robin Uren, Stephen Beecher, Callum R. Smith, and W. Andrew Clarkson

Abstract— **Generation of a donut-shaped first-order Laguerre–Gaussian (LG_{01}) vortex mode via a method designed to yield high mode purity is reported. Our approach utilizes a novel twin-spot end-pumping scheme to directly excite the first order Hermite–Gaussian (HG_{01}) mode in a solid-state laser, followed by a novel astigmatic mode converter based on spherical (concave) mirrors aligned at oblique incidence. A simple theoretical model for the mode converter is derived and from this the design approach is explained along with the potential benefits compared with conventional schemes-based cylindrical-lens astigmatic mode converters, particularly for power scaling. As a proof-of-principle and to confirm the benefits of this scheme in terms of high mode purity we have applied it to an end-pumped Nd:YVO_4 laser to generate a (LG_{01}) beam with a controllable sense of azimuthal phase and hence orbital angular momentum. A method for characterizing the resulting beam-based on analysis of the spiral interference pattern derived with the aid of a Mach–Zehnder interferometer is described and yields a value for the LG_{01} mode purity of 94%. Common sources of mode impurity are identified and the prospects for scaling to higher power whilst maintaining high mode purity are considered.**

Index Terms— **Laser modes, solid lasers.**

I. Introduction

THERE has been considerable interest in vortex modes as their unique properties give them wide ranging applications. Key areas of interest include atom trapping, optical communications, sub-wavelength microscopy and laser processing [1], [2]. Vortex modes are a subset of Laguerre-Gaussian (LG) cavity modes that have a helical phase structure. This is the source of the mode's orbital angular momentum (OAM). Our primary interest is in the area of laser processing of materials, which has attracted considerable attention due to some early experiments demonstrating the production of chiral structures [3] and higher quality laser ablation [4], [5]. However, so far most demonstrations of machining with vortex modes have been limited by the beam quality achievable at high average powers and pulse energies [1], [3], [4]. It is therefore difficult to ascertain with confidence the effect of the OAM on the machining process. This suggests there is a need for a more robust, power scalable technique for generating highly pure vortex modes. It is also essential that this technique be accompanied by a suitable diagnostic capability for determining mode purity. The M^2 parameter, which is a good indicator of the purity of Gaussian fundamental transverse (TEM_{00} or HG_{00}) mode beams, is not sufficient for higher order modes. Quantifying the quality of these modes therefore requires more careful analysis.

There are several popular methods for generating the first order Laguerre-Gaussian (LG_{01}) vortex mode. Direct generation internally within a laser cavity has the potential to yield a very high purity vortex mode. However, in practice, this is rather challenging due to the fact that there are a number of modes with identical transverse intensity distributions including, LG_{01}^{+} modes with clockwise (CW) handedness and LG_{01}^{-} modes with counter-clockwise (CCW) handedness, radially-polarized and azimuthally-polarized modes that do not carry OAM and incoherent combinations of orthogonally orientated (HG_{01}) modes [6]. This makes preferential selection of the desired mode (i.e. LG_{01}^{+} or LG_{01}^{-}), whilst at the same time suppressing unwanted modes extremely difficult. Clearly, a prerequisite for achieving this is a means for discriminating between vortex modes with opposite handedness. The use of annular shaped pump beams [7]–[9] or spot defect mirrors [10], [11] to create matching gain or loss distributions to the desired mode have been employed for direct generation of donut modes, but, for the reasons stated above, cannot guarantee robust operation on a high purity vortex mode. In addition to the use of an annular pump beam, Di Lin *et al.* in [12] exploit the different intracavity standing-wave intensity distributions for LG_{01}^{+} and LG_{01}^{-} vortex modes in a standing-wave laser using two nano-wires inserted into the cavity to differentiate between these modes by virtue of creating a differential loss. This approach, however, has the shortcoming that the nano-wires have to be aligned to subwavelength accuracy to generate the desired mode making practical implementation difficult.

Alternatively, vortex modes can be generated external to the laser using, for example, a spiral phase plate [13], [14] or a liquid crystal spatial light modulator [15] to convert a fundamental laser (HG_{00}) mode into a $LG_{01}^{\pm}$ mode. These schemes have the attraction of being straightforward to implement, but as they only impart an azimuthal phase variation on to the fundamental mode, they have the shortcoming that they do not yield a very pure vortex mode. Moreover, spatial light modulators have rather limited power handling and hence are not suitable for the high powers generally required for applications in laser processing.

Manuscript received March 12, 2019; revised July 9, 2019; accepted July 12, 2019. Date of publication July 25, 2019; date of current version August 21, 2019. The work of R. Uren and C. R. Smith was supported by the Engineering and Physical Sciences Research Council (EPSRC) for studenships. *(Corresponding author: W. Andrew Clarkson.)*

The authors are with the Optoelectronics Research Centre, University of Southampton, Southampton SO17 1BJ, U.K. (e-mail: wac@orc.soton.ac.uk).

Color versions of one or more of the figures in this article are available online at http://ieeexplore.ieee.org.

Digital Object Identifier 10.1109/JQE.2019.2931006

Another approach for producing a vortex mode is to employ an astigmatic mode converter (AMC). This approach was initially proposed by Tamm and Weiss [16] and later expanded upon by M.W. Beijersbergen *et al.* in [17]. The AMC, as conceived in [17], comprises two cylindrical lenses aligned parallel and with respect to an incident beam so to yield an astigmatic region between the lenses. In this way, the Gouy phase shift between orthogonal beam components at 45° to the lens axes over the astigmatic region can be manipulated to allow a high-order Hermite-Gaussian (HG) beam to be converted into a Laguerre-Gaussian (LG) beam or vice versa. The AMC is a popular method for converting a HG_{01} mode into a LG_{01} vortex mode and has been shown theoretically capable of producing vortex modes of very high purity [18]. However, this requires high quality cylindrical lenses, precise alignment and a high quality HG mode. These conditions are not straightforward to satisfy as cylindrical lenses tend to be of poorer quality than spherical optics. Moreover, standard methods for producing HG_{01} modes (e.g. by pump beam offset and mirror misalignment) tend to yield beams with significant mode impurities.

In this paper, we describe a method for generating high purity LG_{01} vortex modes that employs a new design of AMC based on spherical mirrors aligned at oblique incidence in combination with a twin-spot end-pumping scheme to generate a high quality HG_{01} mode. This approach has been applied to an end-pumped Nd:YVO_4 laser and we explore both theoretically and experimentally the impact of misalignment on LG_{01} mode purity. Through careful optimization of the AMC design and alignment we demonstrate an LG_{01} mode purity of >94% and consider measures that could yield a further improvement in mode purity. Finally, we consider merits of our scheme for the generation of high power vortex beams for applications such as laser processing of materials.

II. Theory

We begin by developing the theory for the AMC based on spherical mirrors in order to understand the design criteria, following the approach developed by M.W. Beijersbergen *et al.* in [17] for the cylindrical lens AMC. The electric field for a HG mode may be expressed in Cartesian coordinates x, y and z as

$$E_{HG}(x,y,z) = E_0 \frac{w_0}{w(z)} H_m\left(\frac{\sqrt{2}x}{w(z)}\right) H_n\left(\frac{\sqrt{2}y}{w(z)}\right) \times exp\left(\frac{-\left(x^2+y^2\right)}{w(z)^2}\right) exp\left(\frac{i\pi\left(x^2+y^2\right)}{2\lambda R(z)}\right) \times exp\left(\frac{-i2\pi z}{\lambda}\right) exp\left(i(m+n+1)\zeta(z)\right) \quad (1)$$

where E_0 is a scaling factor, w_0 is the beam radius of the fundamental (HG_{00}) mode at the waist position, x,y are transverse positions, z is the position along the propagation direction from the waist, $w(z)$ is the beam radius at distance z from the waist position, m and n are the mode orders in x and y directions respectively, H_m is the Hermite polynomial of order m, λ is the wavelength, $R(z)$ is the radius of curvature

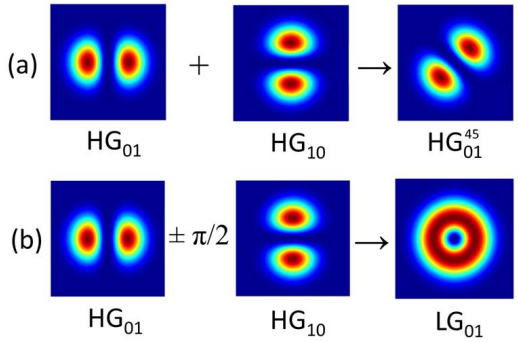

Fig. 1. (a) Schematic showing that a HG_{01} mode orientated at 45° is equivalent to a coherent combination of HG_{01} and HG_{10} modes. (b) Schematic showing that a LG_{01} vortex mode is equivalent to a coherent combination of HG_{01} and HG_{10} modes with a phase difference of $\pi/2$.

of the wavefront at distance z, $\zeta(z)$ is the Gouy phase shift and z_R is the Rayleigh range given by

$$z_R = \frac{\pi w_0^2}{\lambda} \quad (2)$$

The beam radius, $w(z)$ and Gouy phase, $\zeta(z)$ evolve with propagation distance, z, according to

$$w(z) = w_0\sqrt{1+\left(\frac{z}{z_R}\right)^2} \quad (3)$$

$$\zeta(z) = arctan\left(\frac{z}{z_R}\right) \quad (4)$$

Physically the Gouy phase shift represents the phase change, relative to a plane wave, that a transverse mode experiences as it passes through a focus [19]. For a higher order ($HG_{m,n}$) mode and non-astigmatic focusing, the total Gouy phase, $\Psi(z)$, evolves with distance from the beam waist according to

$$\Psi(z) = (m+n+1)\zeta \quad (5)$$

However, for astigmatic focusing with the beam waist in the sagittal plane (y,z) sharing the same position (i.e. at $z=0$) with the beam waist in the tangential plane (x,z) equation (5) should be modified to

$$\Psi(z) = (m+1/2)\zeta_S + (n+1/2)\zeta_T \quad (6)$$

to take into account the different values for the Rayleigh range, z_{RS} and z_{RT}, and hence the different Gouy phase shifts, ζ_S and ζ_T, in the sagittal (S) and tangential (T) planes respectively. The principles of operation of the spherical mirror AMC for the purpose of converting a HG_{01} mode to an LG_{01} vortex mode are illustrated in *Fig. 1* and *Fig. 2*. A HG_{01} beam with its lobes orientated at 45° to the S and T planes, labeled for convenience as a HG_{01}^{45} mode, is incident on the spherical mirror astigmatic mode converter as shown. This beam can be considered as a coherent superposition of HG_{01} and HG_{10} modes as illustrated in *Fig. 1*(a). The spherical mirror mode converter simply comprises two very high reflectivity concave mirrors of equal radius of curvature separated by a distance ($2d$) and aligned so that the beam strikes both at the same angle of incidence (see *Fig. 2*). The incident beam parameters

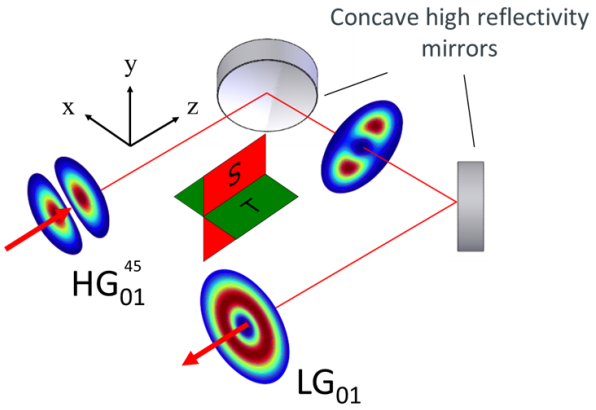

Fig. 2. Diagram of an AMC based on spherical mirrors. Both the coordinate axes and the sagittal, S, and tangential, T, planes are defined as they are used throughout this paper.

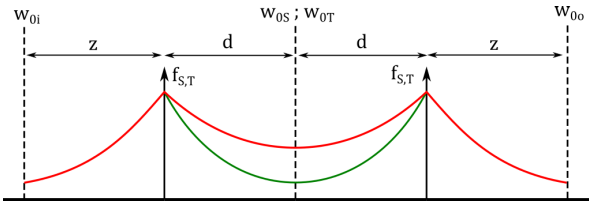

Fig. 3. Schematic showing the evolution of beam radii in the sagittal (red line) and tangential (green line) planes with distance within the spherical mirror AMC. The beam radii in the sagittal and tangential planes are equal before and after the AMC and evolve with distance as shown by the red line.

(i.e. beam waist size and position) are selected so that a beam waist is formed at the mid-point ($z = 0$) of the arm between the two concave mirrors (i.e. at a distance d from each mirror). The combined HG_{01} and HG_{10} beam form different size beam waists, w_{0S} and w_{0T}, in the astigmatic region between the two concave mirrors due to the different focal lengths for the mirrors in the S and T planes that result from the oblique angle of incidence of the beams (see *Fig. 3*). As a result of the symmetrical nature of the AMC, the HG_{01} and HG_{10} beams exiting the final AMC mirror have the same beam parameters (i.e. beam radius and wavefront curvature) as at the input mirror. In the astigmatic region between the two mirrors, the Gouy phase shifts, Ψ_{10} and Ψ_{01}, for the respective HG_{01} and HG_{10} components evolve differently with the result that there is a net phase shift, $\Delta\Psi$, between the beams as they exit the final AMC mirror given by

$$\begin{aligned}\Delta\Psi &= \Psi_{01} - \Psi_{10} = \zeta_T - \zeta_S \\ &= 2\arctan\left(\frac{d}{z_{RT}}\right) - 2\arctan\left(\frac{d}{z_{RS}}\right)\end{aligned} \tag{7}$$

where d is the distance from the beam waist to AMC input (or output) mirror. From (7) it can be seen that $\Delta\Psi$ depends only on the Rayleigh ranges, z_{RT} and z_{RS}, for the beam in the astigmatic region and on the separation of the mirrors. In *Fig. 1*(b) it is shown that an LG_{01} vortex mode is a coherent superposition of HG_{01} and HG_{10} modes with a $\pi/2$ phase difference. Thus, by arranging for $\Delta\Psi = \pi/2$ in (7) we can convert the incident HG_{01}^{45} mode into a LG_{01} vortex mode. Further simplification of (7) reveals that this condition is satisfied when

$$z_{RT} = d\left(\frac{z_{RS} - d}{z_{RS} + d}\right) \tag{8}$$

In order for the beam to be stigmatic outside the AMC, the beam radii in orthogonal S and T planes at the entrance and exit to the AMC (i.e. at $z = \pm d$) must be equal. From (2) and (3) we see that this yields the following relationship between z_{RT}, z_{RS} and d:

$$\frac{z_{RT}^2 + d^2}{z_{RT}} = \frac{z_{RS}^2 + d^2}{z_{RS}}, \tag{9}$$

which can be further simplified to

$$z_{RS} z_{RT} = d^2 \tag{10}$$

From equations (8) and (10) we can then obtain the following expressions for z_{RT} and z_{RS}

$$z_{RT} = d\left(\sqrt{2} - 1\right) \tag{11}$$

$$z_{RS} = d\left(\sqrt{2} + 1\right) \tag{12}$$

We can now apply one final boundary condition, namely, that the radii of curvature of the wavefronts for the beam incident and emerging from the AMC must be equal in both the S and T planes. This leads to the following relation between the radii of curvature of the wavefronts, R_S and R_T, of the beam in the astigmatic region of the AMC immediately adjacent to the concave mirrors in the S and T planes, respectively.

$$\frac{1}{R_i} = \frac{1}{R_S} - \frac{1}{f_S} = \frac{1}{R_T} - \frac{1}{f_T} \tag{13}$$

where R_i is the radius of curvature of the beam incident on the AMC, and f_S and f_T are the focal lengths of the concave mirrors in the S and T planes, respectively. The above expression can be re-written as follows:

$$\Delta D = \frac{1}{f_T} - \frac{1}{f_S} = \frac{1}{R_T} - \frac{1}{R_S} \tag{14}$$

where ΔD is the difference in dioptric power for the concave mirrors in the S and T planes. R_S and R_T are related to the respective Rayleigh ranges, z_{RT} and z_{RS}, by [20]

$$R_S = \frac{d^2 + z_{RS}^2}{d} \tag{15}$$

$$R_T = \frac{d^2 + z_{RT}^2}{d} \tag{16}$$

Substituting (11) and (12) into (15) and (16) and then the resulting expressions into (14) yields the following simple expression relating d to ΔD:

$$d = \frac{1}{\Delta D\sqrt{2}} \tag{17}$$

It is worth noting that the above relation also applies to the more general case where custom-shaped lenses (or mirrors) with different focal lengths in orthogonal planes are used, as well as for the situation of interest here where the difference

in focal lengths in orthogonal planes is derived by employing standard concave high reflectivity mirrors at an oblique angle of incidence. For the case of a cylindrical lens AMC with a focal length, f, (17) reduces to $d = f/\sqrt{2}$ in agreement with the analysis described by M.W. Beijersbergen *et al.* in [17]. For an AMC based on concave mirrors aligned with respect to the beam at an angle-of-incidence, θ, the focal lengths in S and T planes can be written as [21]

$$f_S = \frac{R_c}{2\cos(\theta)} \tag{18}$$

$$f_T = \frac{R_c \cos(\theta)}{2} \tag{19}$$

where R_c is the radius of curvature of the concave mirrors. Substituting (18) and (19) and into (14) yields the following expression relating d to the mirror parameters:

$$d = \frac{R_c}{2\sqrt{2}\sin(\theta)\tan(\theta)} \tag{20}$$

It can be seen from (20) that the design of a spherical mirror AMC is very straightforward given the availability of suitable concave mirrors with high reflectivity dielectric coatings at the desired angle of incidence. One practical point worth mentioning is that relatively large angles of incidence are needed to avoid an excessively long mirror separation. Whilst the design of the AMC is simple, it is crucial that the incident HG_{01}^{45} beam has high purity and has the correct size and wavefront curvature for the chosen AMC design. Substituting (11) or (12) into (3) yields the following expression for the incident beam radius in both the S and T planes:

$$w(d) = \left(\frac{2\sqrt{2}\lambda d}{\pi}\right)^{1/2} \tag{21}$$

Similarly, the following expression for the radius of curvature, R_i, of the beam incident on the AMC can be obtained by substituting (12) and (15) into (13):

$$\frac{1}{R_i} = \frac{1}{2d\left(2+\sqrt{2}\right)} - \frac{1}{f_S} \tag{22}$$

Expressions (21) and (22) yield the required values of the incident beam parameters for the spherical mirror mode converter to yield a pure LG_{01} mode. These can in turn be used to calculate the required beam waist size and its distance from the AMC. It is important to note here the calculation for the beam waist size should take into account the mode order and hence the M^2 parameter for the HG_{01}^{45} beam in orthogonal S and T planes. The use of incorrect incident beam parameters will manifest in an error in the Gouy phase difference and an impure final LG_{01} mode, so care should be taken to provide a suitably tailored input beam. Compared to the cylindrical lens AMC, the spherical mirror AMC has the attractions that fewer components (and optical surfaces) are required leading to lower loss and, hence the potential for use at higher power levels without degradation in mode quality. Moreover, the spherical mirror AMC design is aromatic and hence can be employed over a broad range of wavelengths.

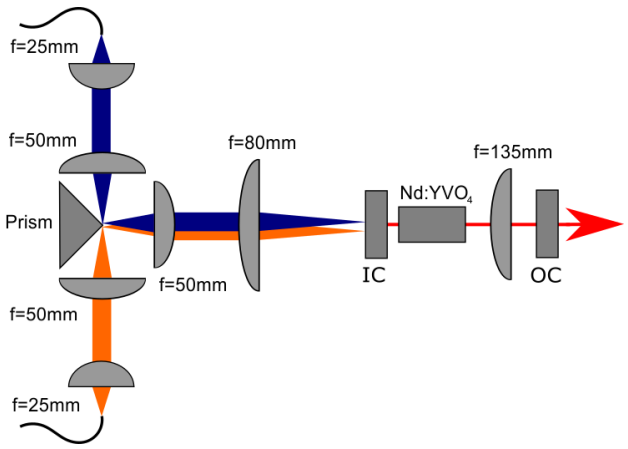

Fig. 4. Schematic of twin-pump-spot diode-end-pumped HG_{01} Nd:YVO_4 laser.

The design of the spherical mirror AMC does not depend on the laser wavelength or spectral bandwidth. However, from (21), it is seen that required incident beam size does have a $\lambda^{1/2}$ dependence implying that there would be a departure in the Gouy phase shift from the optimum value for wide bandwidth laser sources. The result would be some distortion in the output beam, but this would be negligible for lasers with bandwidths less than a few tens-of-nm. It is worth mentioning that higher-order $LG_{0,l}$ OAM modes could also be generated with spherical mirror AMC providing that the appropriate $HG_{m,n}$ modes can be generated with high purity for the input beam.

III. First-Order Hermite-Gaussian Laser

A prerequisite for generating a high quality LG_{01} mode via the AMC is a HG_{01} laser source with high mode purity. In earlier work, HG_{01} modes have been generated directly in a laser by inserting a thin wire into the resonator to suppress lasing on the Gaussian fundamental (HG_{00}) mode [17], [22] or via off-axis laser diode pumping [23], [24]. Both approaches have the shortcoming that they do not provide effective suppression of higher order HG_{mn} modes leading to significant mode impurity. Moreover, the use of off-axis pumping (or equivalently, mirror misalignment in a HG_{00} laser) yields an asymmetric temperature profile and consequent beam distortion at high pump powers making power scaling difficult. We have adopted a different approach in which the inversion distribution has been tailored to provide a high spatial overlap with the desired HG_{01} mode to achieve preferential lasing on this mode. Unwanted modes are suppressed by virtue of having a much poorer overlap with the inversion distribution and hence a higher threshold. This is achieved using an diode-end-pumped Nd:YVO_4 laser configuration with two pump beams adjusted in size and separation to yield an intensity profile in the gain medium that closely resembles that of the HG_{01} mode.

The experimental set-up for the Nd:YVO_4 laser (shown in *Fig. 4*) employs a simple two-mirror cavity configuration comprising a plane input coupler with high reflectivity ($> 99.8\%$) at the lasing wavelength ($1.064\mu m$) and high

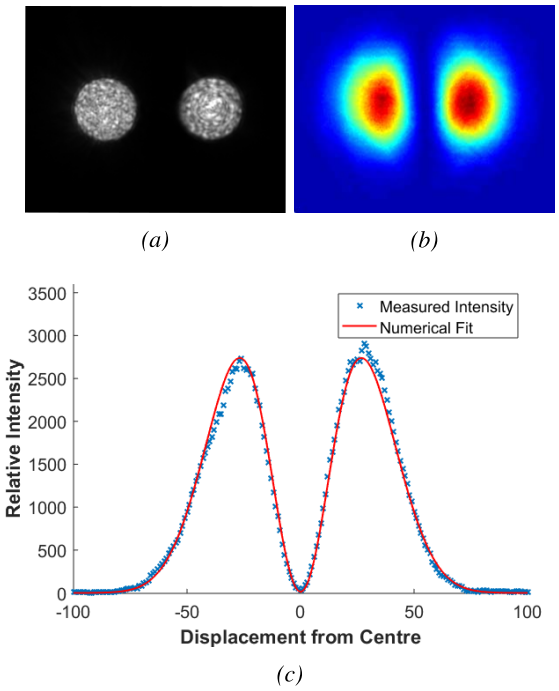

Fig. 5. *(a)* CCD image of the pump beam at the focus, *(b)* CCD image of the resulting HG_{01} laser output, *(c)* Measured intensity profile through the central section of the laser output beam and numerical fit for a perfect HG_{01} mode.

transmission ($> 95\%$) at the pump wavelength ($\sim 808\ nm$), an antireflection coated 5 *mm* long 1 *at.%* doped Nd:YVO_4 crystal, an antireflection coated plano-convex lens with focal length, 135 *mm*, and a plane output coupler with reflectivity, 95% at the lasing wavelength. The Nd:YVO_4 crystal was mounted in a water-cooled copper heat-sink located immediately adjacent to the input coupler, and the resonator length and lens position were adjusted to yield the desired laser mode size. Pump light was provided by two fiber-coupled diode lasers operating at $\sim 808\ nm$. The output from each $105\mu m$ diameter ($0.22\ NA$) delivery fiber was collimated with a 25 *mm* focal length plano-convex lens and then focused with the aid of a 50 *mm* focal length plano-convex lens close to the apex of a knife-edge fused silica 45° prism with high reflectivity coatings at 808 *nm*. The two pump beams were aligned in a counter-propagating collinear fashion as shown in *Fig. 4* yielding reflected pump beams propagating in the same direction, but with a lateral spacing that could be varied by adjusting the prism position. The beams exiting the prism were then relay imaged by a simple telescope comprising plano convex lenses with focal lengths of 50 *mm* and 80 *mm* into the Nd:YVO_4 crystal. This arrangement yields the desired twin spot pump geometry (shown in *Fig. 5*(a)) with each spot having a calculated waist diameter of $336\mu m$ in the Nd:YVO_4 crystal with a center-to-center spacing of $538\mu m$ (i.e. 1.6 times the waist diameter) selected to achieve the optimum overlap with the laser's HG_{01} mode. Each diode pump could be controlled separately allowing for precisely equal power in each pump spot. Nd:YVO_4 was chosen as the gain medium due to its strongly polarized emission properties,

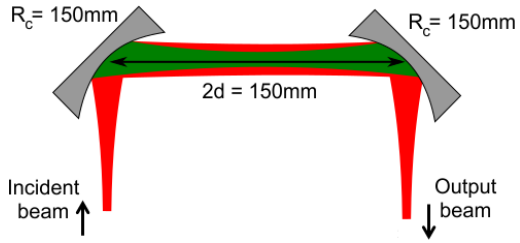

Fig. 6. Schematic of spherical mirror astigmatic mode converter with 150 *mm* radius of curvature mirrors aligned at 45°.

leading to a linearly polarized output without the need of polarization selecting elements, and its short pump absorption length which facilitates mode matching of the pump to the laser mode over the pumped region of the gain medium. The laser resonator was adjusted to give a calculated HG_{00} mode waist diameter of $380\mu m$ on the input coupler (IC), corresponding to calculated HG_{01} mode sizes of $658\mu m$ by $380\mu m$ in orthogonal planes. These mode size parameters were optimized experimentally to yield a high quality HG_{01} output beam (see *Fig. 5*(b)). The HG_{01} laser had a threshold pump power of 224 mW and yielded a maximum output power of $175mW$ at $1064nm$ in a linearly-polarized HG_{01} beam for a combined incident pump power of $\sim 1\ W$. The corresponding slope efficiency was 23% and hence somewhat lower than expected. This was attributed to the losses introduced by the intracavity lens and the non-optimum choice of output coupler mirror. At pump powers below $\sim 1\ W$ the laser yielded a high quality HG_{01} mode output as confirmed by *Fig. 5*(c), which shows intensity profile through the central portion of the CCD camera image shown in *Fig. 5*(b) and the numerical fit to a perfect HG_{01} mode. As pump power was increased beyond $\sim 1\ W$, the output beam became degraded due to thermally-induced phase distortion, so, for the purpose of this study, the pump power was limited to below $\sim 1\ W$. The performance of the spherical mirror AMC with respect to final LG_{01} mode quality is very strongly dependent on the purity of the incident HG_{01} mode. The simple rod-based laser geometry used in our experiments suffers from detrimental thermal effects at modest pump powers. Scaling to higher powers, whilst maintaining high HG_{01} mode purity will require a laser gain medium geometry (e.g. thin disk or thin slab) that offers much weaker thermally-induced beam distortion. With the aid of such a geometry, the twin-spot end pump architecture for generating a pure HG_{01} mode should be scalable to considerably higher powers.

IV. Spherical Mirror Astigmatic Mode Converter

The output beam from the Nd:YVO_4 laser was rotated in the $(x-y)$ plane by 45° with the aid of a dove prism to yield the desired HG_{01}^{45} input beam for the spherical mirror AMC. The latter (shown in *Fig. 6*) comprised two high reflectivity 150 *mm* radius of curvature spherical mirrors aligned at an angle of incidence of 45° for ease of alignment. The mirror spacing was set at 150 *mm* as stipulated by equation (20) and the input beam was aligned with the aid of two steering mirrors and its size adjusted using a telescope (not shown) to

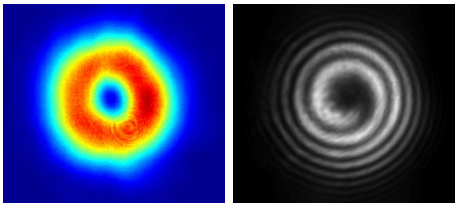

(a) (b)

Fig. 7. *(a)* CCD camera image for the LG_{01}^{-} mode output beam at the waist position after the spherical mirror astigmatic mode converter. *(b)* Spiral interference pattern generated with a Mach-Zehnder interometer.

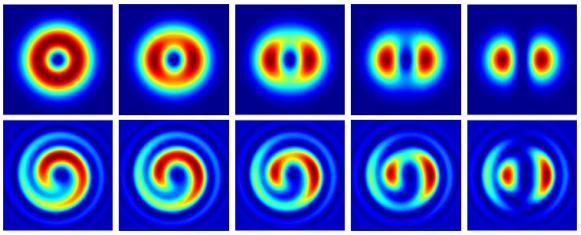

Fig. 8. Theoretical intensity profiles generated by coherently combining HG_{01} and HG_{10} modes with a $\pi/2$ phase difference, where the power level in the LG_{01} for successive images from left to right is 100%, 86%, 66.6%, 40% and 0% respectively of the total beam power (Top row). Corresponding Mach-Zehnder interference patterns (Bottom row).

yield a beam incident on the first AMC spherical mirror with desired beam radius and wavefront radius of curvature. These conditions were achieved by arranging the incident beam to have a waist radius of $202\mu m$ for the HG_{01}^{45} beam in the x and y directions at a position 96 mm away from the first AMC mirror. The LG_{01} output beam from spherical mirror AMC is shown in *Fig. 7(a)* and the overall transmission of the AMC was measured to be $> 99.5\%$. To confirm the presence of OAM we used the standard method of a Mach-Zehnder interferometer [10], [12], [14]. In this scheme the output beam is collimated and split into two beams; one of which is incident on a pin hole to generate a highly divergent spherical wavefront. The two beams are then re-combined with a beam-splitter to form an interference pattern. If the beam incident on the Mach-Zehnder interferometer is a LG_{01}^{+} vortex beam with CW handedness (or an LG_{01}^{-} vortex beam with CCW handedness) then the resulting interference pattern is a spiral, where the handedness of the spiral allows differentiation between CW and CCW handedness. In our experiment, the interference pattern, shown in *Fig. 7(b)*, has a well-defined spiral pattern with CCW handedness confirming the presence of a LG_{01}^{-} beam. It should be noted that a vortex beam with opposite handedness can be produced by rotating the dove prism before the spherical mirror AMC, so that the input HG_{01} beam is orientated at $-45°$ rather than $+45°$. While the output beam from the spherical mirror AMC appears, at first sight, to be a very pure LG_{01} vortex beam, closer inspection of the intensity distribution in *Fig. 7(a)* and the interference pattern in *Fig. 7(b)* reveal that the output beam from the AMC does not have perfect azimuthal symmetry indicating the presence of some mode impurity. Indeed, there are many examples reported in the open literature (see for example [11], [25]) where impurity in generated $LG_{01}^{+/-}$ modes, evident from a lack in azimuthal uniformity of their intensity profiles, can be severe. This raises the problem of how to quantify the purity of these modes with respect to mode content and calls into question the usefulness of diagnostic techniques such as the observation of spiral interference patterns in a Mach-Zehnder interometer as a means to evaluate these beams.

V. Vortex Mode Purity

As stated earlier, an LG_{01} mode can be de-composed into two orthogonal HG_{01} modes that are $\pi/2$ out of phase. It therefore follows that any laser cavity capable of supporting an LG_{01} mode can also support these constituent modes as well. It then follows that these are likely impurities to arise when generating vortex modes via any method internal to a laser cavity. Furthermore, in an AMC, if the input HG_{01} mode is not perfectly orientated at 45° to the sagittal (or tangential) plane of the AMC, or the AMC is misaligned, then some residual HG_{01} mode content will be remain. We have therefore examined how additional HG_{01} mode content influences the spiral interference pattern obtained using a Mach-Zehnder interferometer.

The top row of images in *Fig. 8* show the theoretical intensity profiles derived by a coherently combining HG_{01} and HG_{10} modes with a $\pi/2$ phase difference. The first image depicts the scenario where the power levels for HG_{01} and HG_{10} modes are equal yielding a perfect LG_{01} vortex mode labeled as having 100% LG_{01} mode content. The second, third, fourth and fifth images show the intensity profiles that result from an increasing imbalance in power between the HG_{01} and HG_{10} modes such that the LG_{01} mode purity decreases to 86%, 66.6%, 40% and 0% of the total power, respectively. This simulation would apply to the scenario where the input beam deviates from 45° by increasing angles, showing that the output beam would evolve from a pure LG_{01} mode to a pure HG_{10} mode. The lower set of images in *Fig. 8* show the theoretical interference patterns generated by interfering the beams in the top row with a coherent spherical wave, E_{Sph}, given by (23):

$$E_{Sph} = \left(\frac{1}{r}\right) exp\,(ikr)\,. \tag{23}$$

As expected, the interference pattern for the pure LG_{01} mode has a clear spiral shape and this degrades as the imbalance in power between the constituent HG_{01} and HG_{10} increases. However, it is quite striking that the spiral pattern is still very visible even when the power for the HG_{10} mode is only 40 % of the total power. This simulation clearly shows that the observation of a spiral interference pattern with a Mach-Zehnder interferometer is not a sufficient test for vortex mode purity. The intensity profile for the pure LG_{01} mode and its interference pattern are azimuthally symmetrical. However, for the scenario depicted in *Fig. 8*, where mode impurity arises from an imbalance in power for the constituent HG_{01} and HG_{10} modes, the intensity profile of the resulting output beam and the corresponding interference pattern show increasing azimuthal asymmetry as power imbalance increases.

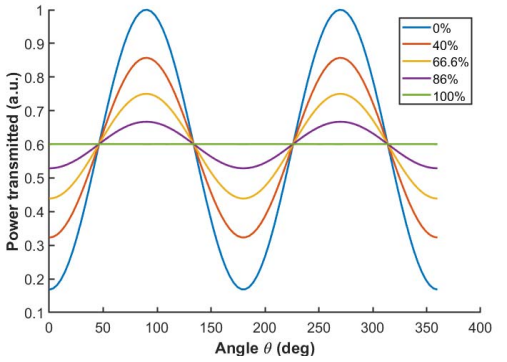

(a)

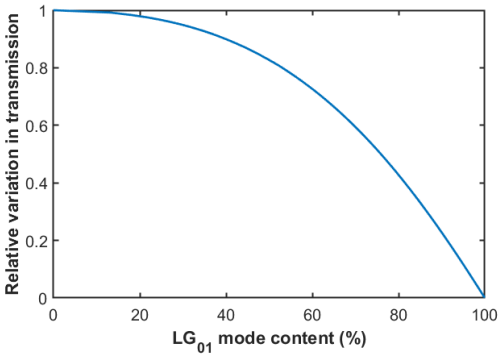

(b)

Fig. 9. (a) Calculated intensity variation versus azimuthal angle, θ, for the interference patterns in *Fig. 8*. (b) Relative intensity variation as a function of LG_{01} mode content.

Thus, analysis of the azimuthal intensity variation can yield quantitative information on LG_{01} mode purity for this common cause of beam distortion. Experimentally, the azimuthal variation in intensity could be measured by, for example, rotating a narrow slit aligned with its axis of rotation at the beam's center and recording the power variation. *Fig. 9(a)* shows the calculated intensity variation as a function of slit azmuthal angle, θ, for the scenarios shown in *Fig. 8*, and *Fig. 9(b)* shows the relative variation in transmitted power versus purity level for the LG_{01}. This approach for characterizing the beam has the attraction that even a relatively low level of mode impurity can be detected. Moreover, this can be used as a diagnostic for optimizing the alignment of the spherical mirror AMC to reduce beam asymmetry due to mode distortion. It is important to note, however, that this method will not reveal undesirable Gaussian HG_{00} mode content as this impurity is azimuthally symmetric. Therefore, its application is limited to systems where HG_{01} mode impurities are the most likely, such as AMCs.

VI. Mode Converter Performance

To evaluate the performance of the spherical mirror AMC and the impact of misalignment on LG_{01} mode purity, the dove prism was adjusted to incrementally change the angle of orientation of the incident HG_{01} mode from it's optimum orientation at 45° to approximately ∼1°. This allowed us to introduce a known amount of excess HG_{01} mode impurity.

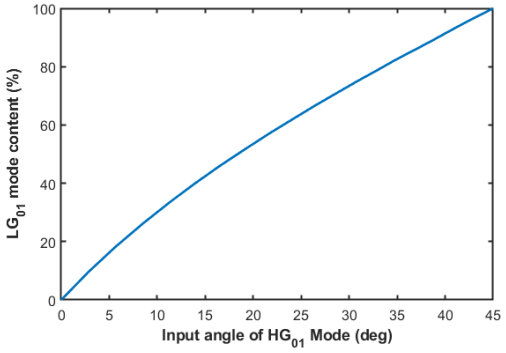

(a)

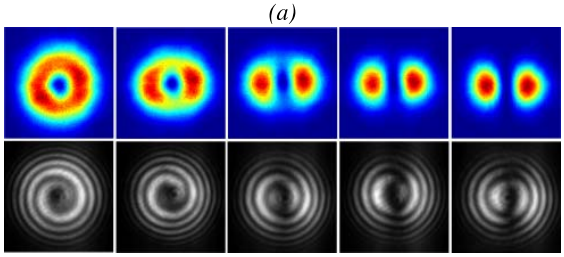

(b)

Fig. 10. *(a)* shows the relation between the input angle of the HG_{01} mode and the expected percentage of LG_{01}^{+} contained in the converted mode. The top row of *(b)* depicts the LG_{01} modes converted from input HG_{01} modes at, from left to right, input angles of 45^o, 39^o, 25^o, 15^o and 1^o. The bottom row shows their corresponding Mach-Zehnder interference patterns.

The theoretical impact on LG_{01} mode purity (i.e. fraction of the power in the desired LG_{01} mode compared to the total power after the AMC) is plotted in *Fig. 10(a)* as a function of HG_{01} orientation from 45°. At each angle, the resulting output beam was evaluated by recording the intensity profile, the Mach-Zehnder interference pattern and, with the aid of a slit mounted on a rotation stage, the azimuthal variation in intensity was measured. We can then estimate the LG_{01} mode content for each HG_{01} orientation from the theoretical curve in *Fig. 10(a)*. Example converted beam images and Mach-Zehnder interference patterns are shown in *Fig. 10(b)*. The modes depicted correspond to approximately, from left to right, 100%, 88%, 63%, 42% and 3% LG_{01} content. These experimental results show that the spiral pattern is clearly discernible, if degraded, even when the output beam has only ∼63% of the power in the LG_{01}. It should be stressed that these are theoretical estimates for the LG_{01} mode content for a perfectly performing AMC with a perfect LG_{01} mode input beam, albeit with an angular misalignment from 45°. Once again the experimental results confirm the need for greater scrutiny when assessing mode purity. The variation in measured azimuthal intensity, shown in *Fig. 11*, can be compared with the theory in *Fig. 9(b)* to gauge the actual level of LG_{01} mode purity for different input angles of the HG_{01} beam. In this case the optimum input angle orientation (i.e. $\theta = 45°$) yields an LG_{01} mode purity of 94%. This assumes that the main source of mode impurity is an imbalance in the powers for the constituent HG_{01} and HG_{10} modes due to imperfect alignment of the incident beam and/or AMC or non-optimum input beam parameters (i.e. beam size and wavefront radius of curvature). This result shows that

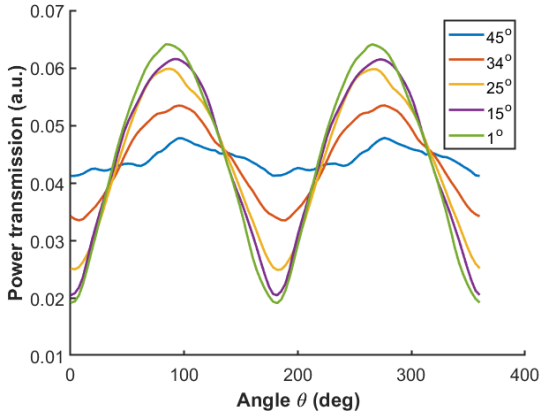

Fig. 11. Azimuthal variation in transmitted intensity for different HG_{01} mode orientations.

high purity LG_{01} vortex beams can be produced by the spherical mirror AMC in combination with a high purity incident HG_{01} beam. Further improvement in LG_{01} mode impurity should be possible through careful optimization of the input beam parameters and AMC alignment to minimize azimuthal variation in intensity.

VII. Conclusions

In summary, we have demonstrated an improved method for generating high purity LG_{01} vortex modes by utilizing a novel twin-spot end pumping scheme to directly generate a high quality HG_{01} mode from a solid-state laser followed by a novel AMC based on spherical mirrors. We have also shown that the standard method for confirming the presence of a vortex mode (i.e. by observation of a spiral interference pattern in a Mach-Zehnder interferometer) does not provide a satisfactory gauge of mode purity and can yield misleading results. To remedy this short coming we have added an additional diagnostic test to measure the azimuthal intensity variation to identify common causes of vortex mode impurity based on a imbalanced contributions from constituent HG_{01} and HG_{10} modes. This approach allows an accurate estimate of vortex mode purity in many situations of practical interest and will prove very useful when assessing the relative merits of different approaches for generating vortex modes. Using this simple diagnostic approach, we have shown that our scheme can yield an LG_{01} vortex mode with very high purity ($\sim 94\%$) and that further improvement in mode purity may be possible via further optimization the AMC and input beam parameters. Furthermore, scaling to high power levels, as required by applications such as materials processing, should be readily achievable by combining this scheme with a disk (or slab) gain medium architecture.

Acknowledgment

The data underpinning this publication is available from the University of Southampton repository at https://doi.org/10.5258/SOTON/D0833.

References

[1] C. Hnatovsky, V. G. Shvedov, W. Krolikowski, and A. V. Rode, "Materials processing with a tightly focused femtosecond laser vortex pulse," *Opt. Lett.*, vol. 35, no. 20, pp. 3417–3419, Oct. 2010.

[2] K. Izumisawa *et al.*, "Crystalline silicon (111) needle formed by optical vortex illumination," in *Proc. Conf. Lasers Electro-Opt. Eur. Eur. Quantum Electron. Conf. (CLEO/Europe-EQEC)*, Jun. 2017, p. 1.

[3] F. Takahashi, K. Miyamoto, H. Hidai, K. Yamane, R. Morita, and T. Omatsu, "Picosecond optical vortex pulse illumination forms a monocrystalline silicon needle," *Sci. Rep.*, vol. 6, no. 1, Feb. 2016, Art. no. 21738.

[4] J. Hamazaki, R. Morita, K. Chujo, Y. Kobayashi, S. Tanda, and T. Omatsu, "Optical-vortex laser ablation," *Opt. Express*, vol. 18, no. 3, pp. 2144–2151, Feb. 2010.

[5] M. Duocastella and C. B. Arnold, "Bessel and annular beams for materials processing," *Laser Photon. Rev.*, vol. 6, no. 5, pp. 607–621, 2012.

[6] I. A. Litvin, S. Ngcobo, D. Naidoo, K. Ait-Ameur, and A. Forbes, "Doughnut laser beam as an incoherent superposition of two petal beams," *Opt. Lett.*, vol. 39, no. 3, pp. 704–707, Feb. 2014.

[7] T. Dietrich, M. Rumpel, T. Graf, and M. A. Ahmed, "Efficient generation of cylindrically polarized beams in an Yb:YAG thin-disk laser enabled by a ring-shaped pumping distribution," *Proc. SPIE*, vol. 9893, Apr. 2016, Art. no. 98930M.

[8] J. W. Kim, J. I. Mackenzie, J. R. Hayes, and W. A. Clarkson, "High power Er:YAG laser with radially-polarized Laguerre–Gaussian (LG_{01}) mode output," *Opt. Express*, vol. 19, no. 15, pp. 14526–14531, Jul. 2011.

[9] J. W. Kim and W. A. Clarkson, "Selective generation of Laguerre–Gaussian (LG_{0n}) mode output in a diode-laser pumped Nd:YAG laser," *Opt. Commun.*, vol. 296, pp. 109–112, Jun. 2013.

[10] Y. Zhao, Q. Liu, W. Zhou, and D. Shen, "~1 mJ pulsed vortex laser at 1645 nm with well-defined helicity," *Opt. Express*, vol. 24, no. 14, pp. 15596–15602, Jul. 2016.

[11] S. Tan, C. Zhou, A. Shirakakwa, K.-I. Ueda, and J. Li, "Vortex Ti:Sapphire laser by using an intracavity spot-defect spatial filter," *Opt. Laser Technol.*, vol. 96, pp. 76–80, Nov. 2017.

[12] D. Lin, J. M. O. Daniel, and W. A. Clarkson, "Controlling the handedness of directly excited Laguerre–Gaussian modes in a solid-state laser," *Opt. Lett.*, vol. 39, no. 13, pp. 3903–3906, Jul. 2014.

[13] M. W. Beijersbergen, R. P. C. Coerwinkel, M. Kristensen, and J. P. Woerdman, "Helical-wavefront laser beams produced with a spiral phaseplate," *Opt. Commun.*, vol. 112, nos. 5–6, pp. 321–327, Dec. 1994.

[14] K. Sueda, G. Miyaji, N. Miyanaga, and M. Nakastuka, "Laguerre–Gaussian beam generated with a multilevel spiral phase plate for high intensity laser pulses," *Opt. Express*, vol. 12, no. 15, pp. 3548–3553, Jul. 2004.

[15] A. Jesacher, A. Schwaighofer, S. Fürhapter, C. Maurer, S. Bernet, and M. Ritsch-Marte, "Wavefront correction of spatial light modulators using an optical vortex image," *Opt. Express*, vol. 15, no. 9, pp. 5801–5808, 2007.

[16] C. Tamm and C. O. Weiss, "Bistability and optical switching of spatial patterns in a laser," *J. Opt. Soc. Amer. B, Opt. Phys.*, vol. 7, no. 6, pp. 1034–1038, Jun. 1990.

[17] M. W. Beijersbergen, L. Allen, H. E. L. O. van der Veen, and J. P. Woerdman, "Astigmatic laser mode converters and transfer of orbital angular momentum," *Opt. Commun.*, vol. 96, nos. 1–3, pp. 123–132, Feb. 1993.

[18] J. Courtial and M. J. Padgett, "Performance of a cylindrical lens mode converter for producing Laguerre–Gaussian laser modes," *Opt. Commun.*, vol. 159, nos. 1–3, pp. 13–18, 1999.

[19] R. W. Boyd, "Intuitive explanation of the phase anomaly of focused light beams," *J. Opt. Soc. Amer.*, vol. 70, no. 7, pp. 877–880, Jul. 1980.

[20] H. Kogelnik and T. Li, "Laser beams and resonators," *Appl. Opt.*, vol. 5, no. 10, pp. 1550–1567, 1966.

[21] A. E. Siegman, *Lasers*. Sausalito, CA, USA: Univ. Science Books, 1986.

[22] A. A. Malyutin and V. A. Ilyukhin, "Generation of high-order Hermite–Gaussian modes in a flashlamp-pumped neodymium phosphate glass laser and their conversion to Laguerre–Gaussian modes," *Quantum Electron.*, vol. 37, no. 2, p. 181, 2007.

[23] T. Ohtomo, S.-C. Chu, and K. Otsuka, "Generation of vortex beams from lasers with controlled Hermite- and Ince–Gaussian modes," *Opt. Express*, vol. 16, no. 7, pp. 5082–5094, Mar. 2008.

[24] S.-C. Chu and K. Otsuka, "Doughnut-like beam generation of Laguerre–Gaussian mode with extremely high mode purity," *Opt. Commun.*, vol. 281, no. 6, pp. 1647–1653, Mar. 2008.

[25] Q. Liu *et al.*, "Integration of helicity-control and pulse-modulation for vortex laser based on a black phosphorus plate," *Opt. Express*, vol. 24, no. 26, pp. 30031–30037, 2016.

Robin Uren received the master's degree in physics from the University of Southampton, Southampton, U.K., in 2014, and the Ph.D. degree from the Optoelectronics Research Centre, University of Southampton, in 2019. He was a member of the Advanced Solid-State Sources Group from October 2014 to September 2018, where his research was primarily focused on realizing high powered vortex modes in solid-state lasers using transverse mode control techniques. This work is the subject of four conference presentations and two pending journal paper submissions.

Stephen Beecher received the B.Sc. (Hons.) degree in physics from the Imperial College London, London, U.K., in 2005, and the joint M.Sc. degree from the University of St. Andrews, Scotland, U.K., and Heriot-Watt University, Scotland, U.K., in 2007. He received the Ph.D. degree in physics from Heriot-Watt University, in 2012. In 2013, he joined the Planar Waveguide and Slab Lasers Research Group, Optoelectronics Research Centre (ORC), University of Southampton, Southampton, U.K. In 2017, he joined Leonardo Company, where he is involved in the development of solid-state laser and non-linear sources.

Callum R. Smith received the master's degree in physics from the University of Southampton, Southampton, U.K., in 2012. He received the Ph.D. degree from the Optoelectronics Research Centre, University of Southampton, in 2017. He is currently a Post-Doctoral with the Fiber Sensors and Supercontinuum Group, Department of Photonics Engineering, Technical University of Denmark, Lyngby, Denmark. His research interests include solid-state lasers, fiber lasers, and microstructured fibers.

W. Andrew Clarkson received the B.Sc. degree in physics from the University of Manchester, U.K., in 1984, and the Ph.D. degree in laser physics from the University of Southampton, U.K., in 1991. He is currently a Professor in optoelectronics with the Optoelectronics Research Centre, University of Southampton, U.K., where he leads the Advanced Solid-State Sources Group. He has authored over 400 conference and journal papers and has filed over 11 patents. His principal research interests include the development of novel coherent light sources with particular emphasis on power-scaling and brightness scaling of fiber and bulk (crystal-based) solid-state lasers and amplifiers. He has served as the Programme Chair and the General Chair for the CLEO/Europe conference and is a fellow of the Optical Society of America.